Eur. Phys. J. A **26**, 135–140 (2005)
DOI 10.1140/epja/i2005-10158-3

THE EUROPEAN PHYSICAL JOURNAL A

Measurement of the G asymmetry for the $\gamma p \rightarrow N\pi$ channels in the $\Delta(1232)$ resonance region

J. Ahrens[7], S. Altieri[11,12], J.R.M. Annand[5], H.-J. Arends[7], R. Beck[7], A. Braghieri[11], N. d'Hose[4], H. Dutz[2], S. Goertz[1], P. Grabmayr[13], S. Hasegawa[10], E. Heid[7], H. Holvoet[3], L. Van Hoorebeke[3], N. Horikawa[10], T. Iwata[9], O. Jahn[7], P. Jennewein[7], R. Kondratiev[8], J. Krimmer[13], M. Lang[7], B. Lannoy[3], K. Livingston[5], J.C. McGeorge[5], W. Meyer[1], A. Panzeri[11,12], P. Pedroni[11,a], T. Pinelli[11,12], I. Preobrajenski[7,8], G. Reicherz[1], G. Rosner[5], M. Rost[7,b], T. Rostomyan[3], D. Ryckbosch[3], M. Schumacher[6], B. Seitz[6], G. Tamas[7], A. Thomas[7], R. van de Vyver[3], Th. Walcher[7], and F. Zapadtka[6]

[1] Institut für Experimentalphysik, Ruhr-Universität Bochum, D-44801 Bochum, Germany
[2] Physikalisches Institut, Universität Bonn, D-53115 Bonn, Germany
[3] Subatomaire en Stralingsfysica, Universiteit Gent, B-9000 Gent, Belgium
[4] CEA Saclay, DSM/DAPNIA/SPhN, F-91191 Gif-sur-Yvette Cedex, France
[5] Department of Physics and Astronomy, University of Glasgow, Glasgow G12 8QQ, UK
[6] II. Physikalisches Institut, Universität Göttingen, D-37073 Göttingen, Germany
[7] Institut für Kernphysik, Universität Mainz, D-55099 Mainz, Germany
[8] INR, Academy of Science, Moscow, Russia
[9] Department of Physics, Nagoya University, Chikusa-ku, Nagoya, Japan
[10] CIRSE, Nagoya University, Chikusa-ku, Nagoya, Japan
[11] INFN, Sezione di Pavia, I-27100 Pavia, Italy
[12] Dipartimento di Fisica Nucleare e Teorica, Università di Pavia, I-27100 Pavia, Italy
[13] Physikalisches Institut, Universität Tübingen, D-72076 Tübingen, Germany

Received: 22 March 2005 / Revised version: 1 September 2005 /
Published online: 31 October 2005 –
Communicated by M. Garçon

Abstract. The G asymmetry of the $\gamma p \rightarrow N\pi$ reaction has been measured for the first time for $E_\gamma = 340 \pm 14$ MeV. This observable, for which very scarce published data exist, plays an important role to disentangle the contributions of the various nucleon resonances. The experiment, performed at the Mainz microtron MAMI, used a 4π-detector system, a linearly polarized, tagged photon beam, and a longitudinally polarized proton target.

PACS. 13.60.Le Meson production – 14.20.Gk Baryon resonances with $S = 0$ – 25.20.Lj Photoproduction reactions

1 Introduction

The determination of the dynamics underlying single-pion photoproduction has been a major challenge in hadronic physics for several decades. However, despite this long history and a large experimental effort, the reaction mechanisms are still far from being understood, mainly because of the contributions from a substantial number of hadronic resonances which are difficult to disentangle ([1,2]).

New perspectives for the study of these resonances have been opened by the possibility of performing experiments using linearly or circularly polarized photons and polarized targets. By careful selection of the new observables, enhanced sensitivities to specific electromagnetic multipoles and, consequently, to a few selected hadronic resonances, are obtained. For example, the measurement of the beam asymmetry (linearly polarized photons and unpolarized target) for both $\gamma p \rightarrow N\pi$ channels [3,4] at photon excitation energies below 450 MeV has allowed a precise determination of the behaviour of the E_{1+} (electric quadrupole) multipole[1] in the $N \rightarrow \Delta$ transition.

[a] e-mail: pedroni@pv.infn.it
[b] As a part of the Diploma thesis.

[1] Here we use the so-called pion multipole notation, where E and M denote the electric or magnetic character of the incoming photon and the indices $l_\pm$ describe the coupling of the pion angular momentum l and the nucleon spin to the total angular momentum $J = l \pm 1/2$.

In the second resonance region (covering excitation energies from $\sim$ 500 MeV to $\sim$ 900 MeV) several overlapping states are present ($P_{11}(1440)$, $D_{13}(1520)$, $S_{11}(1535)$), and this complicates the evaluation of their separate contributions. In this case, the measurement of the helicity dependence (circularly polarized photon beam and longitudinally polarized target) of the $\gamma p \to p\pi^0$ process [5] has been proven to be sensitive to the E_{2-} and M_{2-} partial waves, which strongly couple to the $D_{13}(1520)$ resonance.

A large sensitivity to the M_{1-} partial-wave amplitude and, therefore, to the $P_{11}(1440)$ resonance is given by the double polarization observable G, that can be measured using linearly polarized photons and a longitudinally polarized nucleon target.

The $P_{11}(1440)$ resonance is of particular interest as all its basic parameters (Breit-Wigner mass, decay width and amplitudes) are still very poorly known [6]. This state won recently additional interest due to the signatures of baryon antidecuplet states [7]. In certain models [8], it originates from the mixing of the octet and the antidecuplet states.

The G observable is obtained by flipping the orientation of the linear beam polarization between $+45°$ and $-45°$ with respect to the reaction plane, using a polarized target with polarization vector along the z-axis. It is defined as

$$G = \frac{(\mathrm{d}\sigma/\mathrm{d}\Omega)(45°, z) - (\mathrm{d}\sigma/\mathrm{d}\Omega)(-45°, z)}{(\mathrm{d}\sigma/\mathrm{d}\Omega)(45°, z) + (\mathrm{d}\sigma/\mathrm{d}\Omega)(-45°, z)}.$$

The incoming transverse polarized photon determines the xz plane with the momentum along the z (beam) axis and the polarization vector in the x-direction.

In fig. 1a) the behaviour of G as predicted by MAID (solution MAID2003) [9,10] is plotted as a function of photon energy for the $\gamma p \to p\pi^0$ reaction at $\theta^* = 90°$, where θ^* is the pion angle in the center-of-mass system. The angular behaviour of G for the same reaction at $E_\gamma = 550$ MeV is shown in fig. 1b). In both figures, the full curve represents the standard MAID solution, while the dotted, dashed and dash-dotted curves represent solutions in which the coupling constants of the $P_{11}(1440)$, the $D_{13}(1520)$ and the $S_{11}(1535)$ resonances, respectively, were simply set to zero, without a refit of the experimental data. The difference between the standard and modified solutions indicates the sensitivity of this observable to the different resonances. As is clearly seen in these figures, the influence of the P_{11} resonance is particularly strong, causing even a change of sign of G asymmetry. In contrast, for E_γ below 600 MeV, the sensitivity to D_{13} is much less pronounced, and the sensitivity to S_{11} is almost negligible.

Considering only s- and p-waves, these features can be understood from the multipole expression (see, for instance, [11]):

$$\frac{\mathrm{d}\sigma^0}{\mathrm{d}\Omega} G(\theta^*) = \mathrm{Im}\{M^*_{1-}(E_{1+} - M_{1-}) - 2E^*_{1+}M_{1+}\} \cdot 3\sin^2\theta^* \simeq -\mathrm{Im}M_{1-}\mathrm{Re}M_{1+} \cdot 3\sin^2\theta^*,$$

where $(\mathrm{d}\sigma^0/\mathrm{d}\Omega)$ is the unpolarized differential cross-section. In the approximate equality, we have neglected the effects due to the E_{1+} multipole and to the real part of the M_{1-} multipole. The inclusion of d-waves has no significant effect for $\theta \simeq 90°$ and $E_\gamma < 600$ MeV. Under these kinematical conditions, some additional terms can be neglected due to their dependence on $\cos\theta^*$ and $\cos^2\theta^*$ factors. The remaining terms play a very small role due to their dependence on the imaginary parts of the E_{0+}, E_{2-}, M_{2-}, E_{2+}, and M_{2+} multipoles. G is therefore well suited to extract the parameters of the P_{11} resonance but, for $E_\gamma < 700$ MeV, data for this observable are very scarce for the $\gamma n \to p\pi^+$ channel, and no data exist for the $\gamma p \to p\pi^0$ reaction.

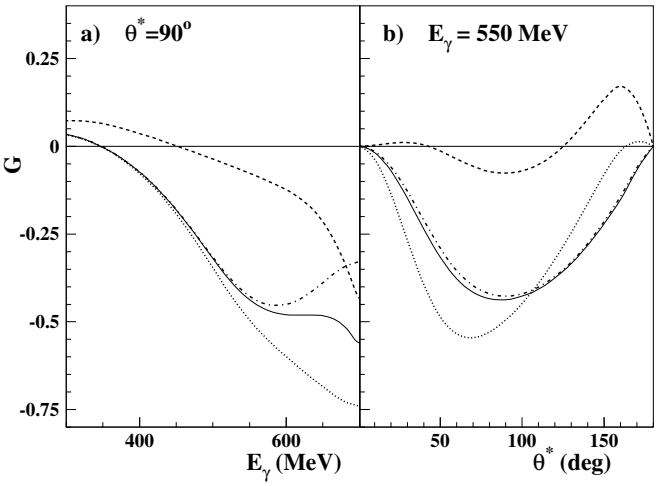

Fig. 1. Energy a) and angular b) dependence of the G observable in the second resonance region for the $\gamma p \to p\pi^0$ reaction as described by the MAID model [9,10]. The curves represent the standard solution (solid line), no $P_{11}(1440)$ (dashed line), no $D_{13}(1520)$ (dotted line), no $S_{11}(1535)$ (dash-dotted line) contribution.

As an introductory step of this study, we present in this paper the first measurement of G for both $\gamma p \to N\pi$ channels at $E_\gamma = 340 \pm 14$ MeV [12]. The data were obtained during a test measurement performed in parallel with the GDH experiment [5,13–17] at the Mainz microtron MAMI, which studied the helicity structure of the partial cross-sections and their contributions to the Gerasimov-Drell-Hearn sum rule. This photon energy value was chosen to get both a maximal cross-section and a high degree of linear photon polarization.

2 Experimental setup

Only the main characteristics of the experimental setup are given here, as the details may be found in refs. [17, 18]. The experiment was carried out at the Glasgow-Mainz tagged photon facility of the MAMI accelerator in Mainz.

Linearly polarized photons were produced by coherent bremsstrahlung of the primary electron beam from a 100 μm diamond crystal collimated by a 3 mm diameter aperture 2.5 m downstream of the diamond. The orientation of the crystal with respect to the beam axis was

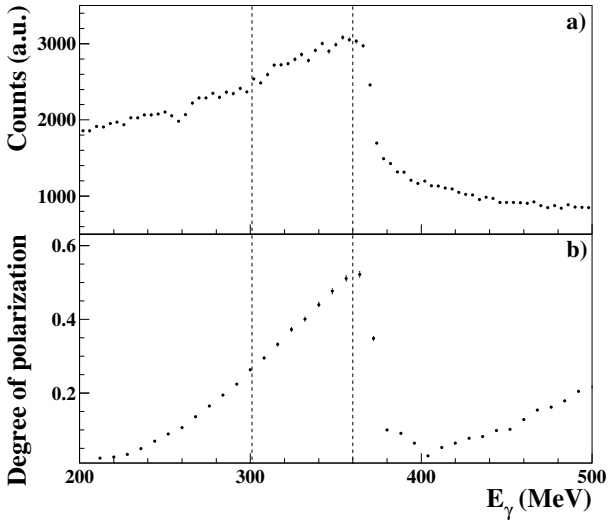

Fig. 2. a) Coherent bremsstrahlung spectrum obtained using a 100 μm diamond crystal. b) The degree of linear polarization as evaluated from the theoretical calculation [20]. In both cases, the two dashed vertical lines define the photon energy region that was used for the analysis. Only statistical errors are shown.

chosen to get a high degree of linear polarization P_γ at photon energies around 340 MeV.

The photon energy was determined by a tagging spectrometer having an energy resolution of about 2 MeV [19]. The tagging efficiency (the probability of a bremsstrahlung photon passing through the collimator given an electron hit in the tagging spectrometer) was continuously monitored during the data taking by an e^+e^--pair detector installed downstream of the main hadron detector. Values of P_γ up to about 50% were obtained at the maximum of the coherent bremsstrahlung peak. P_γ was determined, with a systematic uncertainty of $\pm 3\%$, from the photon spectrum measured by the tagging spectrometer in coincidence with the pair detector and the aid of theoretical calculations [20]. The measured coherent bremsstrahlung spectrum is shown in the upper part of fig. 2, and the evaluated degree of linear polarization is displayed in the lower part of the same figure.

A butanol (C_4H_9OH) frozen-spin target [21] provided the longitudinally polarized protons. The system consisted of a horizontal dilution refrigerator and a superconducting magnet ($\cong$ 2.5 T), which were used in the polarization phase together with a microwave system for dynamic nuclear polarization. During a measurement with beam on target, the polarization was maintained in frozen-spin mode at a temperature of about 50 mK by a magnetic field of 0.4 T, supplied by a small superconducting holding coil inside the cryostat. The proton polarization was measured using NMR techniques with a precision of 1.6%. A maximum polarization close to 88% and relaxation times in the frozen-spin mode of about 200 h were regularly achieved.

Photoemitted hadrons were registered in the large-acceptance detector DAPHNE [22]. DAPHNE is a charged-particle tracking detector covering the full azimuthal angular region and polar angles $\theta_{\rm lab}$ from 21° to 159°. It consists of three cylindrical multiwire proportional chambers, surrounded by segmented plastic scintillator layers and by a scintillator-absorber sandwich. To increase the acceptance for the forward-angle region, the silicon microstrip detector MIDAS [23] and an aerogel Cerenkov counter were installed. MIDAS provided charged-particle tracking and the aerogel suppressed background arising from photoreactions with the atomic electrons.

3 Data analysis

For the results presented here, only the central DAPHNE detector has been used. The identification methods for hadrons detected by the DAPHNE detector have been previously described in detail [17], and only the main characteristics are given here.

The presence of a single charged particle recognized as a proton (pion) was used as a signature of the $p\pi^0$ ($n\pi^+$) channel. Charged particles stopped inside the detector were identified using the range method [24] which is a maximum likelihood algorithm that uses simultaneously all the charged-particle energy losses in the DAPHNE scintillator layers to discriminate between protons and $\pi^\pm$ and determine their kinetic energies. Since at least two energy loss samples along the charged track are needed, the domain of applicability of this method is restricted to particles that penetrate beyond the first scintillator layer.

Charged particles going through all the detector layers could be identified as pions since all recoil protons from π^0 production are stopped within the detectors in the considered E_γ energy interval ($E_\gamma \sim 340$ MeV). Only photoemitted π^+'s can have enough energy to leave the detector but, in this case, it is not possible to determine the pion kinetic energies.

A test run performed prior to the main experiment with an unpolarized liquid-hydrogen target was used for the energy calibration of the detector and for the adjustment of its response to the different particle types. An example of the azimuthal distributions thus obtained for the $n\pi^+$ channel is given in fig. 3a). The solid line is the result of a fit assuming a constant. The low value obtained for the reduced χ^2 of the fit ($\chi^2 = 0.7$) is an indication of the good azimuthal uniformity of the detector response. This value does not improve by adding additional parameters to the fitting function.

A maximum variation of 2% of the response of the different DAPHNE azimuthal sectors was found in this case. Such a value is then taken as a conservative estimate of the systematic-error contribution to the determination of the G asymmetries due to the azimuthal variations in the detection efficiency.

Runs with unpolarized photons were periodically taken during the data taking performed with the polarized target for the control of the stability and the uniformity of the azimuthal detector response.

The unpolarized calibration data were also used to develop and check the offline analysis methods. As

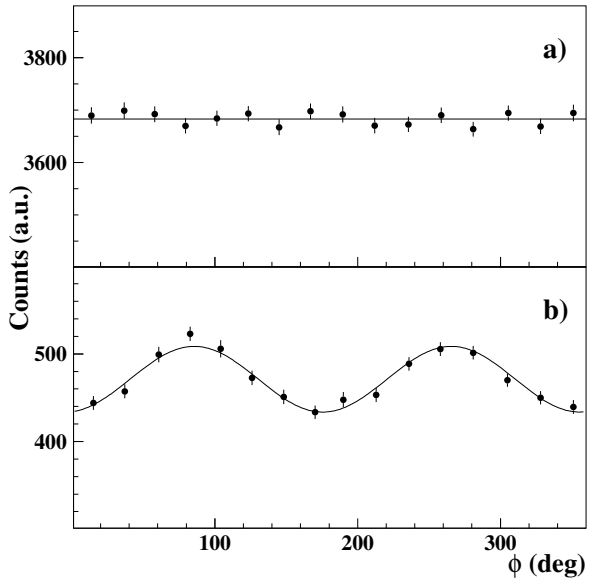

Fig. 3. Azimuthal distribution for $\theta^* = 20°$–$140°$ of the charged pions emitted from the $\gamma p \to n\pi^+$ reaction. a) distribution obtained with an unpolarized beam and an unpolarized target. The solid line shows the constant fit to the distribution. b) Distribution obtained with a linearly polarized beam and a longitudinally polarized target. The solid line shows the 3-parameter fit to the distribution.

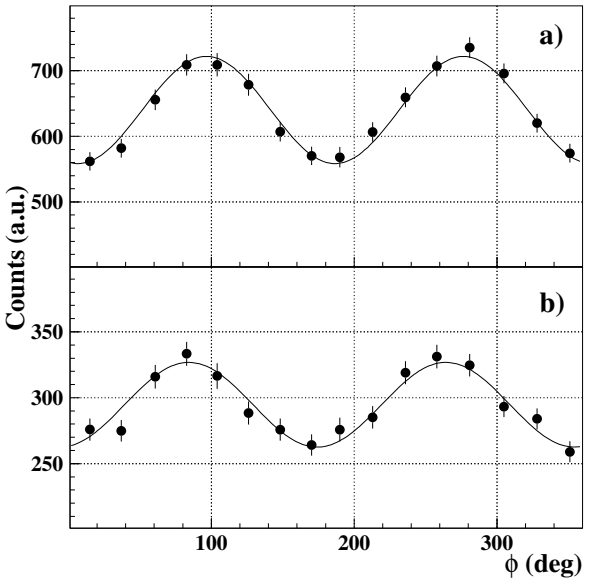

Fig. 4. Azimuthal distribution for $\theta^* = 20°$–$140°$ of the charged pions emitted from the $\gamma p \to n\pi^+$ reaction obtained with a linearly polarized beam and a longitudinally polarized target. The target polarization direction is antiparallel (a)) or parallel (b)) to the photon beam direction.

shown in [17], the measured unpolarized differential cross-sections $(\mathrm{d}\sigma^0/\mathrm{d}\Omega)(\theta^*)$ for the $\gamma p \to N\pi$ channels in the Δ energy region that were thus obtained are in good agreement with previously published data and with the predictions of the models based on multipole analysis. All previous results confirm that the detector response is well understood.

The differential cross-section for the $\gamma p \to N\pi$ process with linearly polarized photons and longitudinally polarized protons is given by the expression:

$$\frac{\mathrm{d}\sigma}{\mathrm{d}\Omega}(\theta^*,\phi) = \frac{\mathrm{d}\sigma^0}{\mathrm{d}\Omega}(\theta^*)\cdot\{1 - p_\gamma \Sigma \cos(2\phi) + p_\gamma p_z G \sin(2\phi)\}\,, \tag{1}$$

where p_γ and p_z are, respectively, the degree of polarization of the photons and protons, and Σ is the photon asymmetry observable for an unpolarized target.

Since DAPHNE has a full ϕ coverage, the G asymmetries were determined, for each θ^* bin, by a simple three-parameter fit of the azimuthal distributions of the detected charged hadrons:

$$N(\theta^*,\phi) = A - B\cos(2\phi) + C\sin(2\phi)\ . \tag{2}$$

The G parameter can then be determined from the fitted A and C coefficients as

$$G = \frac{1}{p_\gamma p_z}\frac{C}{A}\ .$$

An example of the distributions thus obtained for the $n\pi^+$ channel is given in fig. 3.

In order to check the sensitivity to G of the observed distributions, the polarization direction of the target was reversed during the measurement. Since $\sin(2\phi) = \cos[2(\phi - 45°)]$, the effect of this change (see eq. (1)), is to produce a small phase shift between the different experimental azimuthal angular distributions. In fig. 4 the distributions obtained for the $n\pi^+$ channel and with a horizontal orientation of the photon polarization are shown. The target polarization direction is antiparallel (a)) or parallel (b)) to the photon beam direction. In both plots, the continuous lines represent the results of the 3-parameter fit to the distribution. In this case, the fitting function

$$N(\phi) = A' - B'\cos[2(\phi - (C' + 45°)]$$

was used for a better evaluation of the angular shift between the two distributions. It can be easily derived from eq. (2) using basic trigonometric relations. The fitted values of the C' angle are $(+3.3 \pm 0.8)°$ and $(-2.9 \pm 1.2)°$ for plots 4a) and 4b), respectively. The difference between these two values is statistically significant at a level of 4.3 standard deviations.

Data were obtained also with a vertical orientation of the photon beam polarization; similar results for the sensitivity were obtained. The G values separately obtained with the two different beam polarization directions are also in very good statistical agreement among themselves.

Due to the composite nature of the polarized target, the background contribution of the quasi-free $N\pi$ reactions induced on bound protons in C or O nuclei has to be taken into account. This background, coming from spinless nuclei, affects the A coefficient.

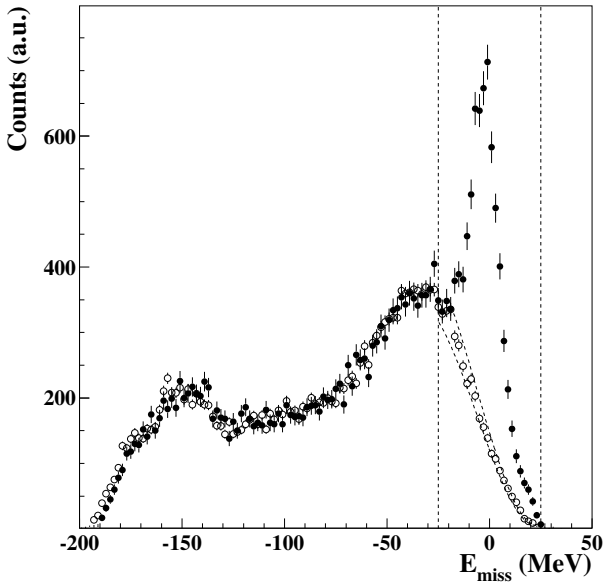

Fig. 5. Missing-energy ($E_{\rm miss}$) spectra for the reaction $\gamma p \to p\pi^0$ under the assumption that the proton originated from a reaction on a free proton. Filled points: butanol target; empty points: pure carbon target. The two dashed vertical lines define the region that was taken into account in the analysis, while the two dashed lines enclose the region defining the uncertainty of the background subtraction.

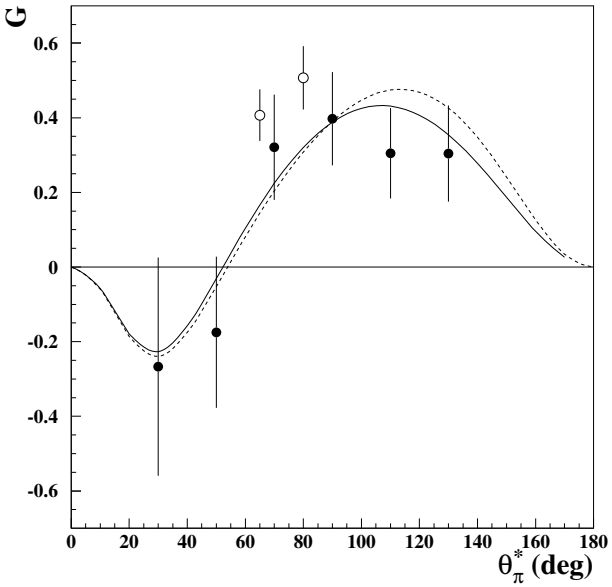

Fig. 6. The measured G asymmetry for the $n\pi^+$ channel is shown as a function of θ^* for $E_\gamma = 340 \pm 14$ MeV (solid points) and compared to the previous data of ref. [27] at $E_\gamma = 350$ MeV. Only statistical errors are shown. The solid (dashed) curves represent the prediction of MAID2003 (SAID-FA04K) multipole analyses.

A partial event-by-event determination of the contribution coming from polarized H nuclei could be performed for the $p\pi^0$ channel using missing energy ($E_{\rm miss}$) [13]. $E_{\rm miss}$ is the difference between the measured proton kinetic energy and the proton kinetic energy evaluated (using E_γ and the polar emission angle) under the assumption that the proton originated from a π^0 production process on hydrogen. The filled points of fig. 5 show the obtained experimental $E_{\rm miss}$ distribution. In the same figure, the open circles represent the same distribution obtained using a pure carbon target. As also shown in ref. [13], the region outside the peak at $E_{\rm miss} = 0$ clearly corresponds to most of the reactions on C and O nuclei, and can be excluded from the analysis.

Denoting with N_H and N_A the number of events, respectively, coming from the free (polarized) and bound (unpolarized) target protons for a given θ^* bin, the G asymmetries can be evaluated using the formula

$$G = \frac{1}{p_\gamma p_z} \frac{C}{A} \frac{(N_A + N_H)}{N_H} \ .$$

The correction factor $R_{\pi^+} = (N_A + N_H)/N_H$ for the $n\pi^+$ channel was evaluated using the measured total cross-section for π^+ production off ^{12}C [25] ($R_{\pi^+} \simeq 3.2$).

For events having $\theta^* < 50^\circ$ there is an additional background source coming from the quasi-free $\gamma n \to p\pi^-$ channel. Under these kinematical conditions the proton can be emitted outside the DAPHNE detector acceptance, and the $\pi^\pm$ separation cannot be performed by our detector. This additional contribution to R_{π^+} was evaluated using a Monte Carlo simulation which incorporates the measured total cross-section for π^- production off ^{12}C [25].

In the case of the $p\pi^0$ channel, the unpolarized carbon data (open circles of fig. 5) were used to determine the fraction of background events ($\sim 20\%$) remaining after the cut in the $E_{\rm miss}$ spectrum. The measured total cross-section for incoherent π^0 production off ^{12}C was then used [26] for the evaluation of the correction factor R_{π^0} ($R_{\pi^0} \simeq 1.4$). The relative systematic error associated with the determination of R is conservatively estimated to be $\pm 10\%$ for the $p\pi^0$ case (band enclosed within the dashed lines of fig. 5) and $\pm 20\%$ for the $n\pi^+$ case.

4 Results and comments

Using the methods described above, the G asymmetry was obtained as a function of the pion c.m.s. angle θ^* for the $\gamma p \to n\pi^+$ and $p\pi^0$ channels at $E_\gamma = 340 \pm 14$ MeV [12]. The results are presented in figs. 6 and 7 for the $n\pi^+$ and $p\pi^0$ channels, respectively, and listed in table 1. The systematic uncertainties contain contributions from azimuthal detector asymmetries (2%), the charged-particle identification method (2.5%), photon polarization (3%), target polarization (0.6%) and background subtraction (10% for $p\pi^0$ and 20 % for $n\pi^+$). The addition of these errors in quadrature leads to a total systematic error of about 11% for the $p\pi^0$ reaction and of about 21% for the $n\pi^+$ reaction.

In fig. 6 two of the four points from ref. [27] for the $n\pi^+$ reaction which comprise the world's published data

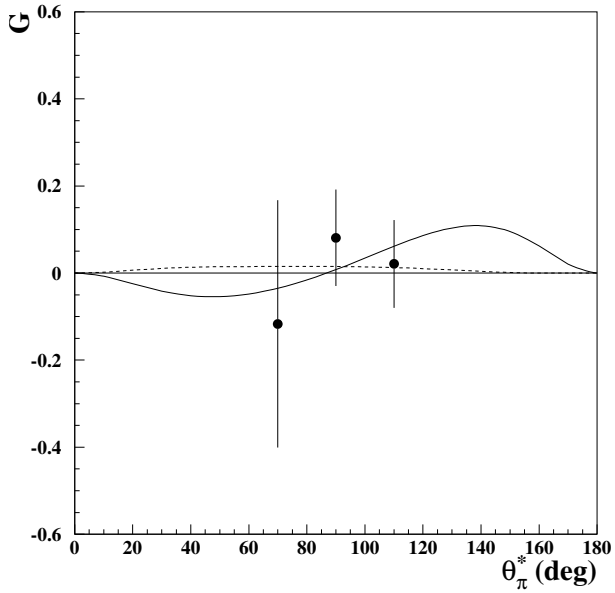

Fig. 7. As in the previous figure but for the $p\pi^0$ channel.

Table 1. Measured G asymmetry values at $E_\gamma = 340$ MeV $\pm$ 14 MeV.

θ^*	$n\pi^+$			$p\pi^0$		
(deg)	G	$\Delta G_{\rm stat}$	$\Delta G_{\rm sys}$	G	$\Delta G_{\rm stat}$	$\Delta G_{\rm sys}$
30	−0.27	±0.29	±0.06			
50	−0.17	±0.20	±0.04			
70	0.32	±0.14	±0.07	−0.12	±0.28	±0.01
90	0.40	±0.12	±0.08	0.08	±0.11	±0.01
110	0.31	±0.12	±0.06	0.02	±0.10	±0.01
130	0.30	±0.13	±0.06			

set below 700 MeV, are also shown. The data are also compared to the predictions of the multipole analyses MAID (solution MAID2003) [9,10] and SAID (solution FA04K) [28]. The measured G asymmetry data are consistent with both predictions but do not have sufficient statistical accuracy to show a preference for either of these models. This agreement is not unexpected since in the Δ resonance region several precise measurements, including those of polarization observables, have been carried out so that the different multipoles have been determined quite well.

A comprehensive study of the G asymmetries for the $\gamma p \to N\pi$ channels will be carried out using the Crystal Ball-Taps large-acceptance detector at the new MAMI-C facility in Mainz [29] which will provide linearly polarized photons up to about 1 GeV.

The authors wish to acknowledge the excellent support of the accelerator group of MAMI. This work was supported by the Deutsche Forschungsgemeinschaft (SFB 201, SFB 443, Schwerpunktprogramm 1034, and GRK683), the INFN (Italy), the FWO Vlaanderen (Belgium), the IWT (Belgium), the UK Engineering and Physical Science Research Council, the DAAD, JSPS Research Fellowship, and the Grant-in-Aid, Monbusho, Japan.

References

1. V.D. Burkert, T.-S.H. Lee, Int. J. Mod. Phys. E **13**, 1035 (2004).
2. B. Krusche, S. Schadmand, Phys. Rep. **51**, 399 (2003).
3. R. Beck *et al.*, Phys. Rev. Lett. **78**, 78 (1997); Phys. Rev. C **61**, 035204 (2000).
4. G. Blanpied *et al.*, Phys. Rev. C **79**, 4337 (1997); **64**, 025203 (2001).
5. J. Ahrens *et al.*, Phys. Rev. Lett. **88**, 232002 (2002).
6. Review of Particle Physics, S. Eidelman *et al.*, Phys. Lett. B **592**, 1 (2004).
7. T. Nakano *et al.*, Phys. Rev. Lett. **91**, 012002 (2003); V.V Barmin *et al.*, Phys. At. Nucl. **66**, 1715 (2003); S. Stepanyan *et al.*, Phys. Rev. Lett. **91**, 0252001 (2003); J. Barth *et al.*, Phys. Lett. B **572**, 127 (2003); A.E. Astratyan *et al.*, Phys. At. Nucl. **67**, 682 (2004); A. Airapetian *et al.*, Phys. Lett. B **585**, 213 (2004); V. Kubarovsky *et al.*, Phys. Rev. Lett. **92**, 032001 (2004); S. Chekanov *et al.*, Phys. Lett. B **591**, 7 (2004).
8. R. Jaffe, F. Wilczek, Phys. Rev. Lett. **91**, 232003 (2003).
9. D. Drechsel *et al.*, Nucl. Phys. A **570**, 580 (1999).
10. D. Drechsel *et al.*, Phys. Rev. D **63**, 114010 (2001).
11. D. Drechsel, L. Tiator, J. Phys. G **18**, 449 (1992).
12. M. Rost, Diplomarbeit, University of Mainz, 2000.
13. J. Ahrens *et al.*, Phys. Rev. Lett. **84**, 5950 (2000).
14. J. Ahrens *et al.*, Phys. Rev. Lett. **87**, 022003 (2001).
15. J. Ahrens *et al.*, Phys. Lett. B **551**, 49 (2003).
16. J. Ahrens *et al.*, Eur. Phys. J. A **17**, 241 (2003).
17. J. Ahrens *et al.*, Eur. Phys. J. A **21**, 323 (2004).
18. S. Wartenberg *et al.*, Few-Body Syst. **26**, 213 (1999).
19. I. Anthony *et al.*, Nucl. Instrum. Methods A **301**, 230 (1991); S.J. Hall *et al.*, Nucl. Instrum. Methods A **368**, 698 (1996).
20. F. Rambo *et al.*, Phys. Rev. C **58**, 489 (1998).
21. C. Bradtke *et al.*, Nucl. Instrum. Methods A **436**, 430 (1999).
22. G. Audit *et al.*, Nucl. Instrum. Methods A **301**, 473 (1991).
23. S. Altieri *et al.*, Nucl. Instrum. Methods A **452**, 185 (2000).
24. A. Braghieri *et al.*, Nucl. Instrum. Methods A **343**, 623 (1994).
25. J. Arends *et al.*, Z. Phys. A **305**, 205 (1982).
26. J. Arends *et al.*, Z. Phys. A **311**, 367 (1983).
27. A. Belayev *et al.*, Sov. J. Nucl. Phys. **40**, 83 (1984).
28. R.A. Arndt *et al.*, Phys. Rev. C **66**, 055213 (2002).
29. R. Beck, L. Tiator, H2 MAMI Proposal, `http://www.kph.uni-mainz.de/SFB443`.